Recursive Simulation Models of the Semiconductor Laser Modulation Characteristics for Accurate Performance Evaluation of Coherent Optical CPFSK Systems

Ioannis Roudas, Yves Jaouën, Jacques Prado, Robert Vallet, and Philippe Gallion, *Member, IEEE*

Abstract—**Modeling of the semiconductor laser nonuniform FM response and residual IM modulation is essential for the computer-aided design of coherent optical communication systems. This paper presents an accurate simulation model, in which the FM and IM responses are represented by recursive digital filters derived directly from measurements. A comparison with previous models of the bibliography reveals the advantages of the current approach. The proposed modeling procedure is applied in the case of a single-electrode DFB laser. This DFB model, in combination with a semi-analytical technique for the evaluation of the error probability, is used to study the influence of the modulation characteristics on the performance of a coherent heterodyne CPFSK system with differential receiver operating at 1 Gb/s. Theoretical and experimental results are in excellent agreement.**

I. Introduction

CONTINUOUS PHASE frequency shift keying (CPFSK) is an attractive modulation format for coherent optical multichannel communication systems [1]. One of its major advantages is that it can be generated directly by injecting a small non-return-to-zero (NRZ) modulation current in the laser.

As light source in the transmitter of coherent optical CPFSK systems, conventional single-electrode and three-electrode distributed feedback (DFB) lasers are most often used.

In the case of single-electrode DFB lasers, the frequency modulation obtained is not ideal [1] because the FM response of these devices is nonuniform [2]. In addition to that there is always a small amount of residual intensity modulation (IM) which coexists with the CPFSK modulation [3]. These two effects cause intersymbol interference (ISI) which degrades the performance of coherent optical CPFSK systems [4]–[7].

In [4]–[7], different models were used to simulate the nonuniform FM response and the residual IM modulation. Jacobsen *et al.* [4] and Caponio *et al.* [5] simulated the FM response by a filter. The residual IM modulation was ignored. Alexander *et al.* [6] and Vodhanel *et al.* [7] used an hybrid approach: 1) the instantaneous amplitude and frequency of the optical signal were calculated at high frequencies by resolution of rate equations; 2) the FM response at low frequencies was simulated by a filter. The diversity of these approaches proves that no standard simulation model exists.

Obviously, modeling depends on the specific application. Here we are interested in a model suitable for computer-aided design of coherent communication systems. From this point of view, the desirable model must be primarily accurate, to enable the calculation of low error probabilities and fast, to enable the simulation of long sequences. For this reason, a compromise must be taken between computing time and sophistication of the model. An abstract, communications engineer oriented model, which does not involve the detailed physical theory of the laser, may therefore be preferable.

This paper proposes a new model with the above features. The principle idea of our approach is that the laser FM response can be approximated by a recursive digital filter derived directly from measurements. The procedure is divided into two steps: 1) measurements of the FM response are fitted by a rational function using a least squares error criterion; 2) the rational function is used to calculate the digital filter coefficients by means of the impulse invariant transformation method. The residual IM response can be also modeled by a recursive digital filter in a similar manner.

This procedure is applied in the case of a single-electrode DFB laser. With this DFB model, we study the impact of the nonuniform FM response on the spectrum, the output waveform and the error probability of a coherent heterodyne CPFSK system with differential receiver operating at 1 Gb/s. The experiment verifies the theoretical results.

The calculation of the error probability is done by a fast and highly accurate semi-analytical technique including both laser phase noise and shot noise.

This is the first time to the authors knowledge that the power penalty caused by the FM and IM responses is calculated accurately for a CPFSK system with differential receiver. A previous attempt on this subject [4] used a simplified model of the FM response in order to derive selection guidelines for the transmitter laser. A more recent analytical study [8] was carried out in the case of wide-deviation FSK system with envelope detection.

Manuscript received November 30, 1994; revised August 11, 1995.

I. Roudas is with Bellcore, Red Bank, NJ 07701 USA.

Y. Jaouën, J. Prado, R. Vallet, and P. Gallion are with the Communications Department, Ecole Nationale Supérieure des Télécommunications, 75634 Paris Cedex 13, France.

IEEE Log Number 9415002.

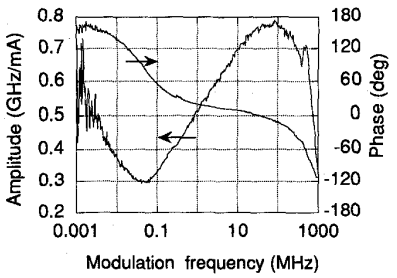

Fig. 1. Measurements of the FM response of a DCPBH DFB laser.

The remainder of this paper is organized as follows. In Section II, the principal models of the FM response are presented and compared to the experiment. In Section III, a new model of the FM response is developed and an application example is given. In Section IV, the model of the IM response is presented. In Sections V and VI, the simulation model and the experimental setup of a coherent heterodyne CPFSK system with differential receiver are described respectively. Finally, in Section VII, the influence of the nonuniform FM response and the residual IM modulation on the system's performance is studied both theoretically and experimentally.

II. FM Response Models

A typical measured FM response of a double-channel planar buried heterostructure (DCPBH) DFB laser is shown in Fig. 1. It presents a magnitude dip in the 1 kHz to 10 MHz region ($f_{\text{dip}} = 40$ kHz) and a phase transition from about 170° to less than 0° as the modulation frequency increases. The slope of the lower side of the dip is equal to −4.2 dB/decade and the slope of the upper side of the dip is equal to 3.3 dB/decade.

The FM response is due to two different mechanisms, the *temperature modulation effect* and the *carrier density modulation effect* [9]. The former dominates at low modulation frequencies and the latter at high modulation frequencies. Under small signal approximation the two effects simply add and the FM response can be written (in terms of the Laplace transform)

$$H(s) = H_c(s) + H_t(s) \tag{1}$$

where $H_c(s), H_t(s)$ denote the carrier and thermal FM contributions respectively. $H_c(s), H_t(s)$ have a phase difference and their vectorial addition results, in general, in an amplitude dip, like in Fig. 1.

Different expressions for $H_c(s), H_t(s)$ are proposed in the bibliography.

A. Carrier FM Response

The transfer function of the carrier induced FM $H_c(s)$ can be derived from the rate equations. For a Fabry-Perot, and approximately for a DFB laser, the carrier FM response is given by [10]

$$H_c(s) = \frac{K_c\left(1 + \dfrac{s}{\omega_g}\right)}{\left(\dfrac{s}{\omega_r}\right)^2 + \dfrac{s}{\omega_d} + 1} \tag{2}$$

where K_c is the FM efficiency of carrier effects in low frequencies, ω_r is the relaxation frequency, ω_d is the damping frequency and ω_g is a frequency related to the gain nonlinearity.

The relation (2) is not valid for DFB lasers which are strongly coupled or have very asymmetric mirror coatings, because spatial hole-burning effects become important [10]. In this case, the transfer function of the carrier induced FM $H_c(s)$ can be evaluated by the model of [11].

B. Thermal FM Response

The transfer function of the thermal FM response $H_t(s)$ can be evaluated by resolution of heat diffusion equations in the chip and the submount [12]. Due to the complexity of the accurate solution, several analytical approximations for $H_t(s)$ are proposed in the bibliography.

The empirical model of Saito *et al.* [13] was shown to describe satisfactorily the behavior of AlGaAs Fabry-Perot lasers with CSP, BH and TJS structure [6], [9]. These lasers display a strong thermal FM efficiency in comparison with their carrier FM efficiency. The thermal FM response is given by

$$H_t(s) = \frac{K_t}{1 + \sqrt{\dfrac{s}{\omega_c}}} \tag{3}$$

where K_t denotes the FM efficiency due to thermal effects and ω_c is the thermal cutoff frequency.

The analytical model of Soundra Pandian-Dilwali [14] was shown to describe well the behavior of DFB lasers. It is based on the study of one-dimensional heat diffusion. The thermal FM response is given by

$$H_t(s) = \frac{2K_t}{3\sqrt{\dfrac{s}{\omega_c}}}\left[\tanh\left(\sqrt{\frac{s}{\omega_c}}\right) + \tanh\left(\frac{1}{2}\sqrt{\frac{s}{\omega_c}}\right)\right] \tag{4}$$

where K_t, ω_c have the same meaning as before.

It is worth noting that at high frequencies $H_t(s) \rightarrow 4K_t/(3\sqrt{s/\omega_c})$, so this model tends asymptotically to the model of Saito *et al.* except for a multiplication factor.

The empirical model of Caponio *et al.* [5] is developed for single electrode InP/InGaAsP DFB lasers with different structures. The thermal FM response is given by

$$H_t(s) = \frac{K_t}{1 + \left(\dfrac{s}{\omega_c}\right)^{1/n}} \frac{1}{1 + \dfrac{s}{\omega_t}} \tag{5}$$

where K_t is the carrier FM efficiency at low frequencies, n is a parameter which usually ranges between 2.5–4, ω_c is the cutoff frequency of the thermal diffusion and ω_t is the cutoff

frequency which accounts for the thermal behavior at high frequencies (~MHz.)

At low frequencies ($f \ll f_t$), the term $(1 + s/\omega_t)^{-1}$ is negligible. At this frequency region, the model of Caponio *et al.* becomes equivalent to the model of Saito *et al.* when $n = 2$. At high frequencies, the term $(1 + s/\omega_t)^{-1}$ makes the thermal FM response to diminish faster than in the two previous models and creates a steeper slope of the upper side of the dip.

C. Comparison of the Thermal FM Response Models

For the comparison of the thermal FM response models, the measurements of Fig. 1 are approximated at low frequencies.

The approximation function is obtained by substituting (2) in (1), and writing $H(s)$ at low frequencies as

$$H(s) \simeq H_t(s) + H_c(0) = H_t(s) + K_c. \tag{6}$$

The least squares algorithm by Levenberg-Marquardt [15] is used for the calculation of the adjustable parameters of $H_t(s)$ in (6).

Fig. 2 (a)–(c) presents measurements (full curves) and their approximation by (6) (dashed curves) for the three different models of $H_t(s)$.

Fig. 2(a) shows that the model of Saito *et al.* approximates well both phase and amplitude dip. However, the slope of the upper side of the dip is not steep enough. Consequently, the theoretical curve intersects measurements at about 10 MHz.

Fig. 2(b) shows that the model of Soundra Pandian-Dilwali approximates well the phase but the amplitude dip is very shallow. This discrepancy indicates that the one-dimensional model of [14], which considers the laser chip as an equivalent single layer with an equivalent planar heat source at the center, is not well adapted to the specific laser geometry.

Fig. 2(c) shows that the model of Caponio *et al.* gives an excellent approximation of both amplitude and phase. On the other hand, the complexity of this model is higher than the complexity of the previous models (four parameters instead of two), and that makes initial conditions more difficult to determine.

Table I summarizes the advantages and drawbacks of the above models. It is worth noting that these observations are based on one specific laser so the conclusions cannot be generalized for all lasers. However, this study indicates the limitations of each model.

From a mathematical point of view, the FM response $H(s)$ can be considered as the transfer function of an analog filter whose input is the laser injection current and whose output is the instantaneous optical frequency.

A problem arises in the computer implementation of all the above models, due to the irrational form of $H(s)$ (i.e., the denominator includes a term $s^{1/n}$). The synthesis of a digital filter representing an irrational transfer function is not trivial [16], [17]. In this case filtering is easier to be performed in the frequency domain by means of the fast Fourier transform (FFT) [5], [8], [18].

On the other hand, the use of FFT inherently assumes that the impulse response of the FM transfer function has finite duration. This is definitely not true. The FM impulse response can be considered as infinite, since its thermal components may vanish very slowly (typically they extend over millions of bits for bit rates at the Gb/s region). This fact suggests that filtering in the time domain with a recursive (IIR, Infinite

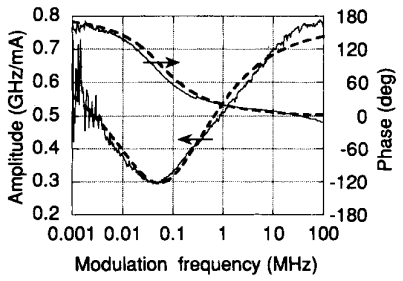

(a)

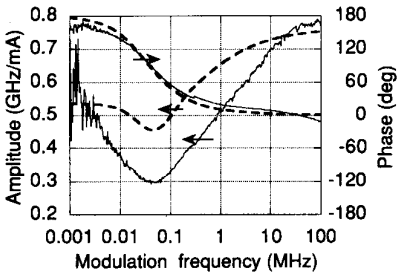

(b)

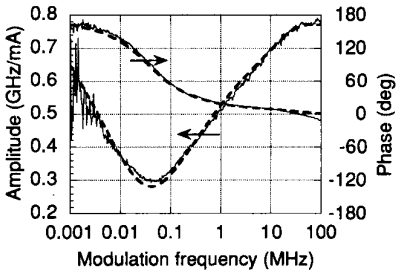

(c)

Fig. 2. Approximation of the measured FM response of the Fig. 1 (full curves) at low frequencies by different models (dashed curves) (a) Model of Saito *et al.* (Parameters: $K_c = 764$ MHz/mA, $K_t = -1.43$ GHz/mA, $\omega_c = 2\pi$ 73 kHz. Only the amplitude of the FM response is approximated). (b) Model of Soundra Pandian-Dilwali (Parameters: $K_c = 764$ MHz/mA, $K_t = -1.7$ GHz/mA, $\omega_c = 2\pi$ 10 kHz. For the calculation of K_t, ω_c the method explained in [14] was used). (c) Model of Caponio *et al.* (Parameters: $K_c = 764$ MHz/mA, $K_t = -1.587$ GHz/mA, $\omega_c = 2\pi$ 37 kHz, $\omega_t = 2\pi$ 32 MHz, $n = 2.32$. Only the amplitude of the FM response is approximated).

TABLE I
ADVANTAGES AND DRAWBACKS OF THE PREVIOUS MODELS FOR THE THERMAL FM RESPONSE

Model	Advantages	Drawbacks
Saito *et al.*	Good approximation of amplitude-phase	Smooth upper side of the dip
Soundra Pandian-Dilwali	Good approximation of the phase	Shallow dip
Caponio *et al.*	Excellent approximation	Difficult initial conditions

Impulse response) digital filter is better adapted to the nature of the specific problem.

It will be shown in the next section that, by choosing a model possessing rational transfer function, the instantaneous optical frequency can be calculated by simple recursive relations with few coefficients.

III. Proposed Model

In this section, we present a new model for the FM response. The FM response is modeled as a recursive digital filter derived directly from measurements.

The design procedure can be divided into two parts, the *approximation* and the *digitization*.

In the following subsections, each part is treated separately.

A. Approximation

The approximation problem can be stated as follows: Given N measurements of the amplitude and phase of the laser FM response $H(s)$, find a rational function $r(s)$ which fits the measurements in the sense of a least squares error criterion.

A suitable set of rational approximation functions $r(s)$ should satisfy the following requirements:

1) Conjugate symmetry around the origin (i. e. $r(s^*) = r^*(s)$). The physical interpretation of this requirement is that the impulse response of the filter should be real.
2) Lowpass behavior (i. e. the order of the denominator polynomial must be greater than the order of the numerator polynomial so that the transfer function of the filter vanishes as $s \to \infty$).
3) Stability (i. e. the poles of $r(s)$ must be located at the left half of the s-plane).

The choice of the form of the approximating function is motivated by the physics of the device. The approximating function $r(s)$ is decomposed in two parts

$$r(s) = r_c(s) + r_t(s) \tag{7}$$

where $r_c(s), r_t(s)$ fit the carrier and thermal FM contributions respectively, each one being adjusted independently and separately.

1) Carrier FM Approximation: The transfer function of the carrier induced FM is assumed to be uniform up to several GHz.

In this case, the parasitics of the laser drive circuit and package limit the laser modulation bandwidth and cause a roll-off at high frequencies as shown in Fig. 1 [19]. Assuming that the parasitics form an equivalent low-pass filter with a series inductance and resistance and a shunt capacitance, $r_c(s)$ can be written in the form

$$r_c(s; a, b, c) = \frac{a}{s^2 + bs + c} \tag{8}$$

where a, b, c are positive real adjustable parameters.

The expression (8) has the form of a minimum phase all-pole causal filter [20], [21]. In consequence, to adjust a, b, c to the measurements, it is sufficient to fit only the amplitude of the FM response since in this case the amplitude and phase are related by the Bayard-Bode relationships [22].

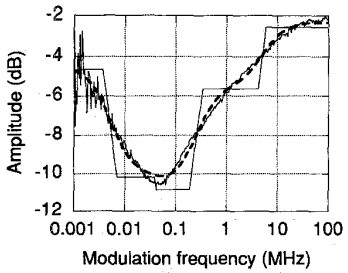

Fig. 3. Amplitude of the measured FM response shown in Fig. 1 (rapidly varying curve) and its approximation by a Bode diagram (staircase curve) for $M = 4$. The approximation by (10) is also given (dashed curve).

2) Thermal FM Approximation: A convenient form for digitization is

$$r_t(s; M, \boldsymbol{r}, \boldsymbol{p}) = \sum_{i=1}^{M} \frac{r_i}{s - p_i} \qquad r_i, p_i \in R, p_i < 0 \tag{9}$$

where the number of fractions M, the residues $\boldsymbol{r}$ and the poles $\boldsymbol{p}$ are adjustable parameters.

This form provides always a very efficient approximation of the thermal FM response. To show this, we can rewrite (7), at the low frequency region (far below the high-frequency roll-off), by use of (8), (9) in the form

$$r(s) \simeq \sum_{i=1}^{M} \frac{r_i}{s - p_i} + \frac{a}{c} = \frac{a}{c} \prod_{i=1}^{M} \frac{s - z_i}{s - p_i} \tag{10}$$

where $\boldsymbol{z}$ are the zeros of $r(s)$ at low frequencies.

The last equality in the expression (10) can be used to make an asymptotic Bode plot (Fig. 3). From this, it is easy to see that by placing a sufficient number of poles and zeros we can create a staircase approximation of the magnitude dip. More particularly, by alternating real poles and zeros, it is possible to create each side of the dip. By placing two successive zeros it is possible to create the bottom of the dip. The major advantage of this method in comparison with [5], [13], [14] is that any dip with arbitrary depth and side slopes can be approximated.

It is worth noting in the expression (9) that, with no loss of generality, only the case of real poles and zeros is considered. This restriction simplifies the calculations and is adopted because it was shown to describe fairly well the behavior of the laser of the Fig. 1. However, the method can be extended in the case of complex poles and zeros.

For the calculation of the parameters $M, \boldsymbol{r}, \boldsymbol{p}$, we approximate the low frequency measurements with $r(s)$ as given by (10). It is necessary to approximate both the magnitude and the phase of the measurements since the zeros of $r(s)$ are not *a priori* in the left half of the s-plane.

Obviously, the approach we adopted for the approximation of the thermal FM response can be extended to approximate also the carrier FM response in the case that the latter is not uniform and the relation (8) does not hold.

B. Digitization

The digitization problem can be stated as follows: given the rational transfer function of an analog filter $r(s)$, find a digital filter with the same characteristics.

Several methods for digitizing an analog filter exist in the literature. We have used a technique called *impulse invariant transformation* [20]. The most attractive property of the impulse invariant transformation is that it preserves both magnitude and phase characteristics of the analog filter by adequate choice of the sampling period T_s.

The straightforward application of the method described in [20] leads to the following procedural steps in order to obtain the frequency recursive relations as follows.

1) Expansion of the carrier FM response (8) in partial fractions

$$r_c(s) = \frac{ih}{s-\sigma+i\Omega} - \frac{ih}{s-\sigma-i\Omega} \tag{11}$$

where

$$h = a/(2\Omega), \quad \sigma = -b/2, \quad \Omega = \sqrt{c-b^2/4}.$$

2) Calculation of the impulse response of (7) by inversion of the Laplace transform of (9), (11)

$$r(t) = \sum_{i=1}^{M} r_i e^{p_i t} + 2he^{\sigma t}\sin(\Omega t) \qquad t \geq 0. \tag{12}$$

3) Calculation of the impulse response of the digital filter $r_d(nT_s)$ by sampling the analog one $r(t)$ at sample intervals T_s

$$r_d(nT_s) \triangleq r(nT_s) = \sum_{i=1}^{M} r_i e^{p_i nT_s} + 2he^{\sigma nT_s}\sin(\Omega nT_s) \qquad n \geq 0. \tag{13}$$

4) Calculation of the z-transform of the digital filter

$$R_d(z) = \sum_{n=0}^{\infty} r_d(nT_s)z^{-n} = \sum_{i=1}^{M} \frac{r_i}{1-e^{p_i T_s}z^{-1}} + \frac{a_1 z^{-1}}{1+a_2 z^{-1}+a_3 z^{-2}} \tag{14}$$

where $a_i, i = 1,\cdots,3$, are related to h, σ, Ω:

$$a_1 = 2he^{\sigma T_s}\sin(\Omega T_s) \tag{15}$$

$$a_2 = -2e^{\sigma T_s}\cos(\Omega T_s) \tag{16}$$

$$a_3 = e^{2\sigma T_s}. \tag{17}$$

5) Calculation of the instantaneous optical frequency $f(nT_s)$ by the following recursive relations

$$f(nT_s) = T_s \sum_{i=1}^{M+1} f_i(nT_s) \tag{18}$$

$$f_i(nT_s) = r_i i(nT_s) + e^{p_i T_s} \times f_i[(n-1)T_s], \quad i = 1,\cdots,M \tag{19}$$

$$f_{M+1}(nT_s) = a_1 i[(n-1)T_s] - a_2 \times f_{M+1}[(n-1)T_s] - a_3 f_{M+1}[(n-2)T_s] \tag{20}$$

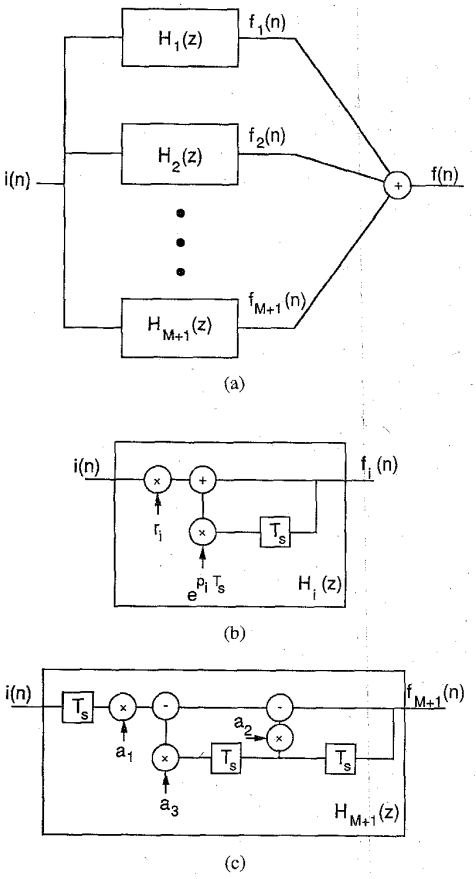

Fig. 4. Digital filter structure.

where $i(nT_s)$ is the instantaneous injection current and $f_i(nT_s), i = 1,\cdots,M+1$, are auxiliary variables for the recursion with $f_i(0) = 0$, $f_i(-T_s) = 0$, $f_{M+1}(-2T_s) = 0$. The scaling factor T_s is added in (18) to compensate the gain induced by the sampling of the analog impulse response in (13) [21]. With this adjustment $R_d(z)|_{z=e^{i\omega T_s}} \approx r(s)|_{s=i\omega}$.

Relations (18)–(20) define a digital filter composed of M first order recursive filters and one second order recursive filter (Fig. 4).

An important property of the approximating functions (8), (9) is that they permit to calculate analytically the $2M+3$ coefficients of the digital filter by the relationships (15)–(20). In consequence, the digital filter is stable because we control the position of poles.

C. Example

The modeling procedure presented in the previous subsections, is used to model the DFB laser of Fig. 1.

First the measurements at the high frequency region ($f \in$ [25 MHz, 1 GHz]) are approximated by (8) using the algorithm of Levenberg-Marquardt (see the Appendix for more details). The values of the adjustable parameters a, b, c are given in Table II.

TABLE II
COEFFICIENTS FOR THE APPROXIMATION OF THE FM RESPONSE AT HIGH FREQUENCIES

a (GHz^3/mA)	18.513
b (GHz)	7.739
c (GHz^2)	24.222

TABLE III
COEFFICIENTS FOR THE APPROXIMATION OF THE FM RESPONSE AT LOW FREQUENCIES BY FIVE PARTIAL FRACTIONS. (CONDITION: FROM TABLE II a/c = 764 MHz/mA).

p_i (2π MHz)	−0.003
	−0.022
	−0.113
	−0.890
	−7.830
z_i (2π MHz)	−0.005
	0.041
	−0.055
	−0.630
	−5.954

TABLE IV
COEFFICIENTS OF THE DIGITAL FILTER DEFINED BY THE RELATIONSHIPS (15)–(20) (T_s = 10 ps)

r_i (GHz MHz/mA)	−0.007
	−0.070
	−0.306
	−1.373
	−12.418
$e^{p_i T_s}$	0.9999998
	0.9999986
	0.9999929
	0.9999441
	0.9995082
a_1 (GHz^2/mA)	0.178
a_2	−1.923
a_3	0.926

Then the measurements at low frequencies ($f \in$ [1 kHz, 60 MHz]) are approximated by (10) for different values of M. The phase approximation is very good even for $M = 3$ but the amplitude approximation presents oscillations which diminish by increasing M and practically vanish for $M = 5$. The poles p_i and the zeros z_i of (10) in the case of $M = 5$ are summarized in Table III.

From the values of the Tables II and III we calculated the 13 coefficients of the recursive filter using the relationships (15)–(20) (Table IV).

In Fig. 5, the amplitude and the phase of the transfer function of the digital filter $R_d(z)|_{z=e^{i\omega T_s}}$ (dashed curves) are plotted together with the measurements (full curves). The sampling rate was chosen equal to 100 GHz in order to avoid aliasing.

To check the validity of the model, the simulated impulse and step response of the digital filter were compared with the theoretical ones and were shown to be in excellent agreement.

IV. MODEL OF THE IM RESPONSE

The injection current causes also a residual IM which coexists with the FM. This is due to the amplitude-phase coupling of the electric field [3] in the laser.

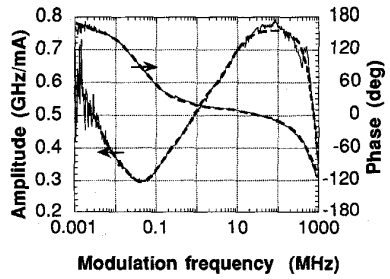

Fig. 5. Measurements of the FM response (full curves) and approximation by the transfer function of the recursive digital filter $R_d(z)|_{z=e^{i\omega T_s}}$ (dashed curves) as a function of the modulation frequency f_m.

The mathematical expression for the amplitude of the electric field of the emitted signal is [3]

$$|E_s(t)| = A\sqrt{1 + my(t)} \tag{21}$$

where A is the unmodulated amplitude of the electric field and m is the IM index defined as

$$m = \frac{I_m}{I_0 - I_{\text{th}}} \tag{22}$$

where I_m is the amplitude of the modulation current, I_0 is the DC bias current and I_{th} is the threshold current.

In (21) $y(t)$ is a function specifying the current modulation and can be written

$$y(t) = h_{\text{IM}}(t) * h_P(t) * i_n(t) \tag{23}$$

where $h_{\text{IM}}(t)$ is the impulse response of the IM response, $h_P(t)$ is the impulse response of the laser parasitics and $i_n(t)$ is the normalized instantaneous modulation current with amplitude ± 1. The operator $*$ denotes convolution.

From the relationship (22) we note that the IM index m increases with the increase of the amplitude of the modulation current I_m. The value of I_m is determined in order to obtain a prescribed frequency deviation.

For example, for a bit rate R_b = 1 Gb/s and for an FM index $0.5 < h < 1$, the frequency deviation ranges from 0.25–0.5 GHz. For the laser of the Fig. 1 the amplitude of the modulation current necessary to obtain these frequency deviations is always $I_m < 1$ mA. Given that for this particular laser $I_0 - I_{\text{th}} \simeq 50$ mA, the IM index m is less than 2% for all FM indices. Hence, the amplitude of the optical signal can be considered as constant.

However, for other laser types (i.e., single-electrode MQW DFB lasers) which present a low FM efficiency, the amplitude of the modulation current necessary to obtain the desired frequency deviations may take important values. Therefore, it is instructive to study the hypothetical case of strong residual IM. This can be done in the following manner: assuming that the cutoff frequency of the laser parasitics is small in comparison with the relaxation oscillation, the IM response can be considered flat and in consequence, $h_{\text{IM}}(t) \simeq \delta(t)$. The laser parasitics are modeled by the second order filter (8) and we can write $h_P(t) = r_c(t)$. Then the amplitude of the complex envelope of the transmitted signal can be evaluated from (21) by replacing $y(t) = r_c(t) * i_n(t)$.

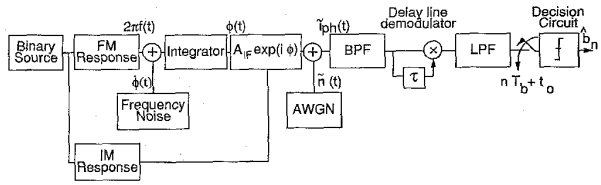

Fig. 6. Block diagram of the simulation model [Abbreviations used: AWGN = additive white Gaussian noise, BPF = bandpass filter, LPF = lowpass filter, τ = delay, t_0 = optimum sampling instant within a bit period ($t_0 \in \{0, T_b\}$)].

V. Simulation Model for a Coherent Optical CPFSK System with Differential Receiver

A block diagram of the computer model of a coherent optical CPFSK system with differential receiver operating at 1 Gb/s is shown in Fig. 6. The input data consists of a pseudo-random binary sequence of variable length (periods varying from "1010$\cdots$" (square wave) to $2^{15}-1$). The sequence represents a non-return-to-zero (NRZ) current of amplitude I_m which is injected into the laser. The instantaneous amplitude and optical frequency are calculated using the models of Sections III and IV.

It is well known [23] that the instantaneous optical frequency of a semiconductor laser presents fluctuations $\dot{\phi}(t)$. The frequency fluctuations $\dot{\phi}(t)$ are simulated as a white Gaussian noise with two side power spectral density equal to $2\pi\Delta\nu$, where $\Delta\nu$ is the 3-dB spectral linewidth. This modeling does not take into account the $1/f$ noise behavior at low frequencies and the laser resonance peak. The sum $2\pi f(t) + \dot{\phi}(t)$ is integrated by use of the trapezoidal rule to obtain the instantaneous phase $\phi(t)$ of the transmitted optical signal.

Fiber and polarization dispersion and fiber nonlinearities are not included in the model. The local oscillator is assumed to introduce negligible phase noise.

The microwave current after the photodiode resulting by the mixing of the received and the local oscillator optical signals, can be written in equivalent baseband signal notation as

$$\tilde{i}_{ph}(t) = A_{\text{IF}}(t) \exp\left\{ i \int_0^t [2\pi f(t') + \dot{\phi}(t')]\, dt' \right\} + \tilde{n}(t) \tag{24}$$

where $A_{\text{IF}} = 2R\sqrt{P_s(t)P_{lo}}$, R is the responsivity of the photodiode, $P_s(t) = |E_s(t)|^2 = A^2[1 + my(t)]$ is the received optical power from the transmitter, P_{lo} is the received optical power from the local oscillator and $\tilde{n}(t)$ is the sum of shot and thermal noises, which can be approximated as an additive white Gaussian noise (AWGN). Tilde denotes the complex envelope of the signals.

In Fig. 6 the transmitter, the local oscillator and the photodiode do not appear like separate units. The program generates directly the signal given by the relation (24).

The bandpass filter (BPF) bandwidth is chosen large in comparison to the signal bandwidth. Thus the only contribution of the bandpass filter is to reduce the AWGN noise. Its influence on the signal and the phase noise is negligible.

For the lowpass filter (LPF), two different filter types were used: 1) a Tscebycheff I with 6 poles, passband ripple 0.1 dB and bandwidth 0.8 R_b; 2) an ideal LPF with very large bandwidth which eliminates the second harmonic after the microwave mixer but does not affect the signal and the phase noise at the output of the receiver. The former was used to plot the output waveforms of the Fig. 9 because it was shown to closely approximate the LPF used in the experiments. The latter was used in the evaluation of the error probability. In this way, the ISI induced only by the FM and the IM responses can be studied.

The differential delay was chosen equal to $\tau = T_b/2$ (T_b = bit duration). This is the optimum value of the delay for an FM index $h = 1$ when the laser's FM response is flat [24]. However, this is not the case when the FM response is nonuniform. In order to optimize the system's performance, the amplitude I_m of the injection NRZ current was modified until the achievement of a maximum eye opening at the output of the receiver for a square wave.

The degradation of the system's sensitivity in prior works is estimated by calculation of the eye closure penalty at the receiver output [25]. In a more accurate approach, the error probability must be used as performance criterion. For the evaluation of the error probability we used a semi-analytical technique [26]. According to this method, the signal is simulated in the absence of noise in order to compute the distortion induced by the nonuniform FM response. The nonuniform FM response changes the phase difference $\Delta\theta_n$ between the two entries of the microwave mixer. The residual IM changes the instantaneous signal-to-noise ratio ρ_0, ρ_1 at the entries of the microwave mixer. Then we can use the relation (9) of Jacobsen *et al.* [4] to evaluate the conditional error probability $P_{e|n}$ of the nth bit of the sequence

$$\begin{aligned} P_{e|n} = \frac{1}{2} - \frac{1}{2}\sqrt{\rho_0\rho_1}e^{-(\rho_0+\rho_1/2)} \sum_{k=0}^{\infty} \frac{(-1)^k}{2k+1} e^{-(2k+1)^2\pi\Delta\nu\tau} \\ \times \left[I_k\left(\frac{\rho_0}{2}\right) + I_{k+1}\left(\frac{\rho_0}{2}\right)\right]\left[I_k\left(\frac{\rho_1}{2}\right) + I_{k+1}\left(\frac{\rho_1}{2}\right)\right] \\ \times \cos\left[(2k+1)\Delta\theta_n\right] \end{aligned} \tag{25}$$

where $I_k(x)$ are the modified Bessel functions of the first kind and $\Delta\nu$ is the 3-dB spectral linewidth of the transmitter.

The total error probability can then be estimated by averaging over all the output samples L

$$P_e = \frac{1}{L}\sum_{n=1}^{L} P_{e|n} \tag{26}$$

where L denotes the sequence length.

The current semi-analytical approach differs from the one proposed by Jacobsen *et al.* [4] in the following two points: 1) it uses more accurate models for the FM and IM responses; 2) it takes into account the ISI caused by the whole sequence and not only by the parts where several repeated marks or spaces occur. It was already used with success for the study of the influence of the BPF on the system's performance [27], [28].

For the simulations, we used TOPSIM [29], a software package for simulation of analog and digital communication systems.

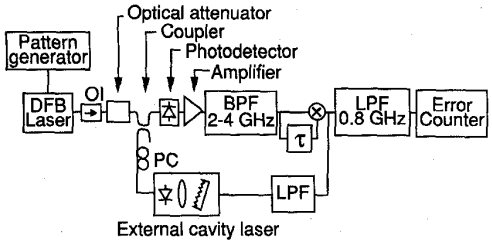

Fig. 7. Experimental setup (Abbreviations used: OI = Optical Isolator, PC = Polarization controller, BPF = bandpass filter, LPF = lowpass filter, τ = delay).

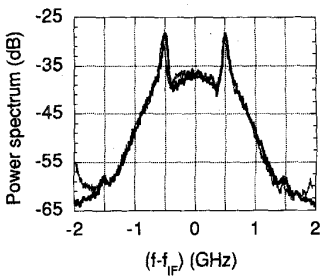

Fig. 8. Theoretical (bold curve) and experimental (thin curve) spectra of the CPFSK.

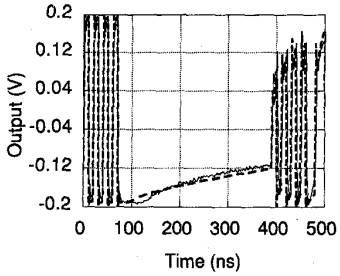

Fig. 9. Theoretical (dashed curve) and experimental (full curve) output waveform of the differential receiver.

VI. Experiment

For the verification of the theoretical evaluations, the experimental arrangement shown in Fig. 7 was employed [28]. The DCPBH DFB laser diode of the Fig. 1 was used in the CPFSK transmitter. Its wavelength was 1520 nm and its 3-dB linewidth for the bias current chosen was about 29 MHz. The laser was directly modulated at a bit rate $R_b = 1$ Gb/s and the optical signal was launched into a single-mode fiber. An optical isolator providing more than 60 dB isolation was used at the laser output to avoid undesired feedback.

A tunable 10 kHz-linewidth external cavity laser was used as local oscillator. The local oscillator power received at the photodetector was $P_{lo} = -5.3$ dBm. This power was not sufficient to produce shot noise limited operation and the contribution of the thermal noise was significant. A polarization controller was used to match the state of polarization of the two lasers. The two optical fields were combined with an 1 : 1 fiber coupler and detected by a PIN photodiode. The photodiode bandwidth was 13 GHz and its responsivity $R = 0.8$ A/W. The IF frequency was fixed at 3 GHz. The IF signal was amplified by a three stage wide-band preamplifier. After the first stage of amplification, the signal was filtered by a bandpass filter with 3-dB bandwidth $B_{\text{IF}} = 2$ GHz. The delay-line discriminator had a 3 GHz zero crossing and delay $\tau = T_b/2$. The lowpass filter (LPF) had a 3-dB cutoff frequency equal to $0.8R_b$.

As for the simulation, the amplitude of the modulation current was adjusted to achieve a maximum eye opening at the output of the receiver for a square wave.

VII. Results and Discussion

In Fig. 8 we compare theoretical (bold curve) and experimental (thin curve) spectra of the CPFSK. In the case of an ideal CPFSK modulation with FM index $h = 1$, in the absence of phase noise, the spectrum consists of a central lobe $3R_b$ large and two impulses located at $\pm R_b/2$ around the central frequency [30]. The effect of the nonuniform FM response is that the impulses are smeared (partly because of the phase noise) and the separation between the central and the secondary lobes has disappeared. Note that the spectra are slightly asymmetric around the IF. This is due to the residual IM of the optical signal which enhances the spectrum at lower frequencies [3]. The peak at the lower left corner of the experimental spectrum is due to the direct detection. Direct detection is not taken into account in the simulation because it is filtered by the bandpass filter.

Comparison between theoretical (dashed curve) and experimental (full curve) waveforms at the output of the differential receiver is shown in Fig. 9. The transmitted sequence contains 320 consecutive zeros at a bit rate $R_b = 1$ Gb/s. Obviously, the nonuniform FM response causes a reduction of the amplitude of the output signal whenever a long sequence of consecutive 1 or 0 is transmitted.

Fig. 10(a)–(c) shows eye-diagrams for three different sequences (square wave, $2^7 - 1$ and $2^{13} - 1$, respectively) in the absence of phase noise and with an ideal lowpass filter with very large bandwidth. The eye opening is normalized, i.e. it is equal to 1 in the absence of ISI. The eye-diagram closes as the sequence length increases. The corresponding power penalty according to the method of [25] is negligible for the square wave, 0.24 dB for the sequence $2^7 - 1$ and 0.59 dB for the sequence $2^{13} - 1$.

Fig. 11 shows the estimated probability of error as a function of the signal-to-noise ratio for three different sequences (square wave, $2^7 - 1$, and $2^{15} - 1$) in the absence of phase noise. The sensitivity penalty at 10^{-9} in comparison with the ideal DPSK receiver (SNR = 13 dB) is negligible for the square wave, 0.4 dB for the sequence $2^7 - 1$ and 0.8 dB for the sequence $2^{15} - 1$.

It should be mentioned here that the method of [25] gives a fast estimation of the power penalty in the absence of phase noise. When phase noise is not negligible, the predictions of [25] do not hold since phase noise is not taken into account in the calculations.

The influence of the residual IM is negligible for the laser of Fig. 1 but in general, it can deteriorate furthermore the performance of the system.

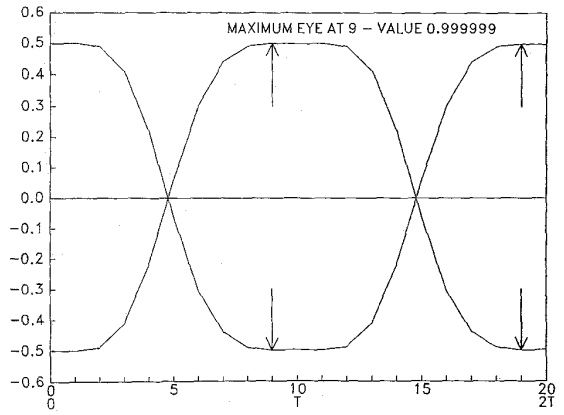

(a)

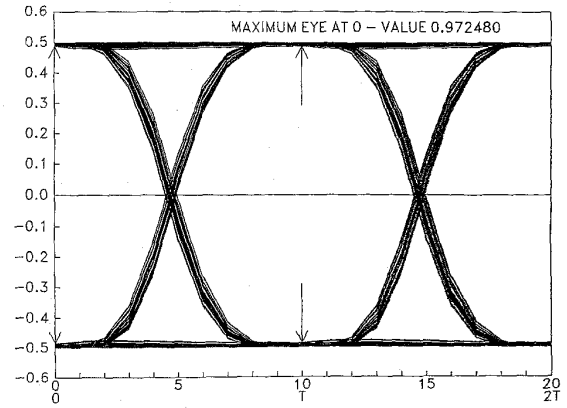

(b)

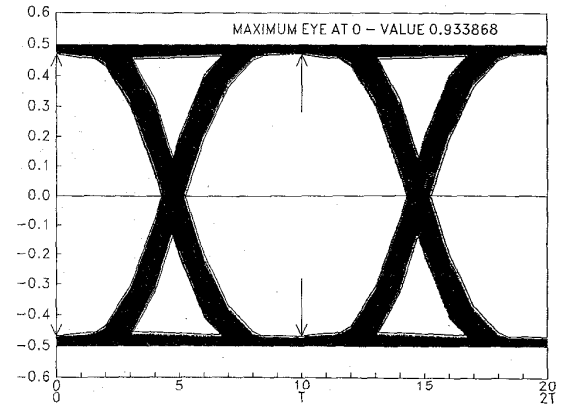

(c)

Fig. 10. Eye-diagrams for different sequences (a) Square wave, (b) $2^7 - 1$, (c) $2^{13} - 1$.

The distortion induced by the combined action of the nonuniform FM response of Fig. 1 and a hypothetical strong residual IM on the eye-diagram is illustrated on the Fig. 12. The transmitted sequence has a period $2^7 - 1$. The IM index is assumed $m = 0.3$. We note that the eye-diagram becomes asymmetric [compare with the Fig. 10 (b)]. Approximately,

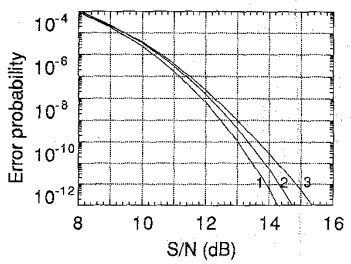

Fig. 11. Influence of the sequence length on the probability of error (Symbols used: Curve 1: Square wave, Curve 2: $2^7 - 1$, Curve 3: $2^{15} - 1$). Condition: IM index $m = 0.02$.

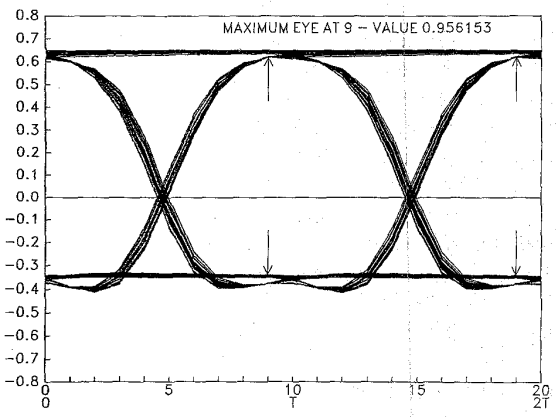

Fig. 12. Eye-diagram for the hypothetical case of an IM index $m = 0.3$.

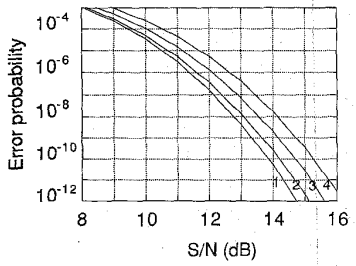

Fig. 13. Combined influence of the nonuniform FM response of Fig. 1 and a hypothetical strong residual IM on the probability of error for a sequence of period $2^7 - 1$ (Symbols used: Curve 1: $m = 0.02$, Curve 2: $m = 0.1$, Curve 3: $m = 0.2$, Curve 4: $m = 0.3$).

the level of the output signal is enhanced by a multiplication factor $(1 + m)$ for the "1" and decreased by a factor $(1 - m)$ for the "0." For example, in Fig. 10 (b) the output signal varies between circa $[-0.5, 0.5]$ and in Fig. 12 the level of the output signal varies between circa $[-0.35, 0.65]$.

The penalty induced by a strong IM modulation can be calculated by the semi-analytical technique of the Section V. Fig. 13 shows the estimated probability of error as a function of the signal-to-noise ratio for three different IM modulation indices ($m = 0.1, 0.2, 0.3$) for a sequence $2^7 - 1$ in the absence of phase noise. For comparison, the curve 2 of Fig. 11 is plotted ($m = 0.02$). From Fig. 13 we conclude that the IM induced penalty at 10^{-9} is less than 1 dB for $m \leq 0.25$.

The above results show that the proposed technique for the modeling of the IM and nonuniform FM responses, together with an accurate semi-analytical method for the evaluation of the error probability, can be a very efficient tool in the computer-aided design of the coherent optical systems.

The semi-analytical method is very general and permits to incorporate other effects as well, like chromatic dispersion and signal distortions due to filtering in the study.

A drawback of the model is that it does not take into account the FM response dependence on the bias current and temperature [2], [9]. However, this dependence is small when the transmitter laser is current and temperature stabilized and in a first approximation can be neglected.

In addition, the model does not take into account the change of the FM response due to the aging of the transmitter laser. In a recent study [31], it is shown that spectral linewidth and FM efficiency of single and three-electrode MQW DFB lasers increase slightly with laser age but this effect, under normal operating conditions, becomes significant only after more than 10^5 hours of continuous operation. Therefore, bit error rate degradation versus time can be assumed negligible with a good degree of accuracy.

The model is applied here only in the case of a single-electrode DFB laser. It was not possible to do the same for other types of lasers, due to the lack of components in ENST facilities. In addition, the application of the modeling procedure to a small and rather insignificant laser sample, was not considered as especially useful, since the form of the FM response can vary significantly from one laser to the other, even for lasers with the same geometry [2].

However, it is possible to do some remarks concerning the robustness of the modeling procedure. As explained by use of a Bode diagram in Fig. 3, expression (9) is very general and allows a staircase approximation to any given set of FM response measurements. The only practical constraint is that the number of fractions M in (9) must be chosen sufficiently low in order to guarantee the convergence of the Levenberg-Marquardt algorithm, which otherwise becomes very slow or stops at local minima. This is a major problem of all optimization algorithms. Convergence is achieved only if the initial conditions are close enough to the true solution. In order to overcome this problem, it is possible to split the approximation part of the modeling procedure, into two steps: 1) a rational interpolating function (Padé approximant [32]) is found which passes from some of the measured points; 2) the Padé approximant can be used as initial condition to the Levenberg-Marquardt algorithm.

VIII. Conclusion

This paper presents an accurate simulation model of the nonuniform FM response and residual IM modulation of semiconductor lasers for coherent optical CPFSK systems design.

According to our approach, the FM and IM responses are represented by recursive digital filters derived directly from measurements. The instantaneous amplitude and frequency are simulated in an elegant manner by recursive relations with very few coefficients which can be calculated analytically. Other important models of the bibliography are discussed and a comparison with the experiment reveals their limitations.

The modeling procedure is applied in the case of a conventional DFB laser. The influence of the nonuniform FM response on the spectrum, the waveform at the output of the receiver, and the error probability of a coherent optical CPFSK system is studied both theoretically and experimentally. The hypothetical case of strong IM response is also examined by eye diagrams and error probability evaluation. The excellent agreement between theoretical and experimental results confirms the validity of the approach.

Appendix
Least Squares Approximation of the Measured FM Response

To approximate N measurements of the FM response $H(\omega_i), i = 1, \cdots, N$, by a function $r(s)|_{s=i\omega}$, it is necessary to define an error function E (Euclidean norm in R^N)

$$E = \sum_{i=1}^{N} r_i^2 = \boldsymbol{r}^T \boldsymbol{r} \tag{27}$$

where $\boldsymbol{r}$ are column vectors with elements r_i defined as follows:

- Amplitude approximation only (at high frequencies)

$$r_i = \frac{||H(\omega_i)|| - ||r_c(\omega_i; a, b, c)||}{\sigma_{||H||}}. \tag{28}$$

- Simultaneous approximation of amplitude and phase (at low frequencies)

$$r_i = \left[\left(\frac{||H(\omega_i)|| - ||r(\omega_i; M, \boldsymbol{z}, \boldsymbol{p})||}{\sigma_{||H||}} \right)^2 + \left(\frac{\phi_H(\omega_i) - \phi_r(\omega_i; M, \boldsymbol{z}, \boldsymbol{p})}{\sigma_\phi} \right)^2 \right]^{1/2}. \tag{29}$$

If the measurement errors are normally distributed with variances $\sigma^2_{||H||}, \sigma^2_\phi$ respectively, the functions $r_c(\omega_i; a, b, c), r(\omega_i; M, \boldsymbol{z}, \boldsymbol{p})$ that minimize the error function E in (27) are shown to be the maximum-likehood approximations of the measurements [15].

The minimization of (27) is a nonlinear least-squares problem. For its resolution the algorithm of Levenberg-Marquardt was used [15]. This algorithm makes use of the first derivative of the error function (27), which is expressed in terms of the Jacobian matrix $J(x)_{ij} = 2r_i \partial r_i(x)/\partial x_j$, where x_j are the variables to be optimized.

In our case, the Jacobian can be calculated analytically. For the shake of completeness, the derivatives $\partial r_i(x)/\partial x_j$ are given below.

A. Amplitude Approximation Only

From the relation (8) the amplitude of the FM approximation is given by

$$||r_c(\omega; a, b, c)|| = \frac{a}{[\omega^4 + (b^2 - 2c)\omega^2 + c^2]^{1/2}}. \tag{30}$$

From (28), (30) it is straightforward to see that

$$\frac{\partial r_i}{\partial a} = -\frac{||r_c(\omega_i)||}{a} \tag{31}$$

$$\frac{\partial r_i}{\partial b} = \frac{||r_c(\omega_i)||b\omega_i^2}{\omega_i^4 + (b^2 - 2c)\omega_i^2 + c^2} \tag{32}$$

$$\frac{\partial r_i}{\partial c} = \frac{||r_c(\omega_i)||(c - \omega_i^2)}{\omega_i^4 + (b^2 - 2c)\omega_i^2 + c^2}. \tag{33}$$

B. Simultaneous Approximation of Amplitude and Phase

From the last equality of the expression (10) the amplitude and the phase of the FM approximation are given by

$$||r(\omega; M, \boldsymbol{z}, \boldsymbol{p})|| = \frac{a}{c}\prod_{i=1}^{M}\left[\frac{\omega^2 + z_i^2}{\omega^2 + p_i^2}\right]^{1/2} \tag{34}$$

$$\phi_r(\omega; M, \boldsymbol{z}, \boldsymbol{p}) = \sum_{i=1}^{M}\left[-\tan^{-1}\left(\frac{\omega}{z_i}\right) + \tan^{-1}\left(\frac{\omega}{p_i}\right)\right]. \tag{35}$$

From (34) and (35), it is straightforward to see that

$$\frac{\partial||r(\omega)||}{\partial z_k} = \frac{z_k||r(\omega)||}{z_k^2 + \omega^2} \tag{36}$$

$$\frac{\partial||r(\omega)||}{\partial p_k} = -\frac{p_k||r(\omega)||}{p_k^2 + \omega^2} \tag{37}$$

$$\frac{\partial\phi_r}{\partial z_k} = \frac{\omega}{z_k^2 + \omega^2} \tag{38}$$

$$\frac{\partial\phi_r}{\partial p_k} = -\frac{\omega}{p_k^2 + \omega^2}. \tag{39}$$

Finally, from (29) we obtain

$$\begin{aligned}\frac{\partial r_i}{\partial\begin{Bmatrix} z_k \\ p_k \end{Bmatrix}} = &-\frac{1}{r_i}\left(\frac{||H(\omega_i)|| - ||r(\omega_i; M, \boldsymbol{z}, \boldsymbol{p})||}{\sigma^2_{||H||}}\right) \\ &\cdot\frac{\partial r(\omega_i)}{\partial\begin{Bmatrix} z_k \\ p_k \end{Bmatrix}} \\ &-\frac{1}{r_i}\left(\frac{\phi_H(\omega_i) - \phi_r(\omega_i; M, \boldsymbol{z}, \boldsymbol{p})}{\sigma^2_\phi}\right) \\ &\cdot\frac{\partial\phi_r(\omega_i)}{\partial\begin{Bmatrix} z_k \\ p_k \end{Bmatrix}}.\end{aligned} \tag{40}$$

ACKNOWLEDGMENT

The authors wish to thank Mr. E. Papproth for providing the measurements of Fig. 1.

REFERENCES

[1] R. A. Linke and A. H. Gnauck, "High-capacity coherent lightwave systems," *J. Lightwave Technol.*, vol. 5, no. 11, pp. 1750–1769, Nov. 1988.

[2] P. Gambini, N. P. Caponio, M. Puleo, and E. Vezzoni, "Accurate measurement of the FM response in magnitude and phase of different DFB laser structures," *SPIE Coherent Lightwave Commun.*, Boston, vol. 1175, pp. 12–23, Sept. 1989.

[3] H. Olesen and G. Jacobsen, "A theoretical and experimental analysis of modulated laser fields and power spectra," *IEEE J. Quantum Electron.*, vol. QE-18, no. 12, pp. 2069–2080, Dec. 1982.

[4] G. Jacobsen, K. Emura, T. Ono, and S. Yamazaki, "Requirements for LD FM characteristics in an optical CPFSK system," *J. Lightwave Technol.*, vol. 9, no. 9, pp. 1113–1123, Sept. 1991.

[5] N. Caponio, P. Gambini, M. Puleo, and E. Vezzoni, "Impact of DFB-LD FM response distortion, in amplitude and phase, on FSK coherent systems," CSELT Tech. Rep., vol. 19, no. 5, pp. 313–316, Nov. 1991.

[6] S. B. Alexander, D. Welford, and D. vL. Marquis, "Passive equalization of semiconductor diode laser frequency modulation," *J. Lightwave Technol.*, vol. 7, no. 1, pp. 11–23, Jan. 1989.

[7] R. S. Vodhanel, A. F. Elrefaie, M. Z. Iqbal, R. E. Wagner, J. L. Gimlett, and S. Tsuji, "Performance of directly modulated DFB lasers in 10 Gb/s ASK, FSK, and DPSK lightwave systems," *J. Lightwave Technol.*, vol. 8, no. 9, pp. 1379–1386, Sept. 1990.

[8] S. P. Majumder, R. Gangopadhyay, and G. Prati, "Effect of line coding on heterodyne FSK optical systems with nonuniform laser FM response," *IEE Proc. Optoelectron.*, vol. 141, no. 3, pp. 200–208, June 1994.

[9] S. Kobayashi, Y. Yamamoto, M. Ito, and T. Kimura, "Direct frequency modulation in AlGaAs semiconductor lasers," *IEEE J. Quantum Electron.*, vol. QE-18, no. 4, pp. 582–595, Apr. 1982.

[10] T. L. Koch and U. Koren, "Semiconductor lasers for coherent optical fiber communications," *J. Lightwave Technol.*, vol. 8, no. 3, pp. 274–293, Mar. 1990.

[11] P. Vankwikelberge, F. Buytaert, A. Franchois , R. Baets, P. I. Kuindersma and C. W. Fredriksz, "Analysis of the carrier-induced FM response of DFB lasers: Theoretical and experimental case studies," *IEEE J. Quantum Electron.*, vol. 25, no. 11, pp. 2239–2253, Nov. 1989.

[12] M. Ito and T. Kimura, "Stationary and transient thermal properties of semiconductor laser diodes," *IEEE J. Quantum Electron.*, vol. QE-17, no. 5, pp. 787–795, May 1981.

[13] S. Saito, O. Nilsson, and Y. Yamamoto, "Coherent FSK transmitter using a negative feedback stabilized semiconductor laser," *Electron. Lett.*, vol. 20, no. 17, pp. 703–704, Aug. 1984.

[14] G. S. Pandian and S. Dilwali, "On the thermal FM response of a semiconductor laser diode," *IEEE Photon. Technol. Lett.*, vol. 4, no. 2, pp. 130–133, Feb. 1992.

[15] W. Press, B. Flannery, S. Teukolsky, and W. Vetterling, *Numerical recipes*, 2nd ed. Cambridge, U.K.: Cambridge Univ. Press, 1992.

[16] L. S. Shieh and C. F. Chen, "Analysis of irrational transfer functions for distributed-parameter systems," *IEEE Trans. Aerosp. Electron. Syst.*, vol. AES-5, no. 6, pp. 967–973, Nov. 1969.

[17] G. E. Carlson and C. A. Halijak, "Approximation of fractional capacitors $1/s^{1/n}$ by a regular Newton process," *IEEE Trans. Circ. Theory*, vol. CT-11, pp. 210–213, June 1964.

[18] D. Marcuse, "Computer Simulation of FSK laser spectra and of FSK-to-ASK conversion," *J. Lightwave Technol.*, vol. 8, no. 7, pp. 1110–1122, July 1990.

[19] R. S. Tucker, "High-speed modulation of semiconductor lasers," *J. Lightwave Technol.*, vol. LT-3, no. 6, pp. 1180–1192, Dec. 1985.

[20] L. R. Rabiner and B. Gold, *Theory and application of digital signal processing*. Englewood Cliffs, NJ: Prentice-Hall, 1975.

[21] A. V. Oppenheim and R. W. Schafer, *Digital signal processing*. Englewood Cliffs, NJ: Prentice-Hall, 1975.

[22] M. Bellanger, "Traitement numérique du signal: Théorie et pratique," in *Collection CNET-ENST*. Paris, France: Masson, 1981.

[23] L. G. Kazovsky, "Impact of laser phase noise on optical heterodyne communication systems," *IEEE Opt. Commun.*, vol. 7, no. 2, pp. 66–78, 1986.

[24] N. Ekanayake, "On differential detection of binary FM," *IEEE Trans. Commun.*, vol. COM-32, no. 4, pp. 469–470, Apr. 1984.

[25] A. F. Elrefaie, R. E. Wagner, D. A. Atlas, and D. G. Daut, "Chromatic dispersion limitations in coherent lightwave transmission systems," *J. Lightwave Technol.*, vol. 6, no. 5, pp. 704–709, May 1988.

[26] M. C. Jeruchim, "Techniques for estimating the bit error rate in the simulation of digital communication systems," *IEEE J. Select. Areas Commun.*, vol. SAC-2, no. 1, pp. 153–170, Jan. 1984.

[27] I. Roudas, Y. Jaouën, and P. Gallion, "Optimum IF filter bandwidth for coherent optical heterodyne CPFSK differential receivers," in *CLEO'94*, Anaheim, May 1994, paper CThI33.

[28] Y. Jaouën, I. Roudas, and P. Gallion, "Experimental reduction of phase-noise influence for an optical CPFSK system with I. F. filtering,"

Microwave and Opt. Tech. Lett., vol. 6, no. 16, pp. 903–905, Dec. 1993.
[29] V. Castellani, M. Pent, G. Taricco, and R. De Gaudenzi, "TOPSIM-IV: An advanced versatile user-oriented software package for computer-aided analysis and design of communication systems," *ESA J.*, vol. 16, pp. 135–158, 1992.
[30] J. G. Proakis, *Digital Communications*. New York: McGraw-Hill, 1989.
[31] M. Fukuda, F. Kano, T. Kurosaki, and J. Yoshida, "Spectral aspect of degradation in 1.55 μm long-cavity MQW DFB lasers," *IEEE Photon. Technol. Lett.*, vol. 4, no. 4, pp. 305–307, Apr. 1992.
[32] G. A. Baker and P. Graves-Morris, *Padé approximants part II: Extensions and applications*. Reading, MA: Addison-Wesley, 1981, pp. 11–12.

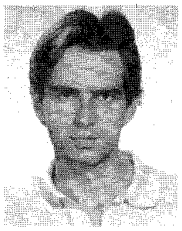

Ioannis Roudas was born in June 1966, in Athens, Greece. He received the Diploma in physics from the University of Athens, Greece in 1988, and the M.S. and Ph.D. degrees from ENST Paris, France, in 1991 and 1995, respectively.

His Ph.D. dissertation at ENST Paris, France concerned modeling and optimal design of coherent optical communication systems. Since 1995, he has been with Bellcore, Red Bank, NJ, where he is currently working on the modeling of multiwavelength optical networks.

Yves Jaouën was born in September 1958 in Quimper, France. He received the DEA and Ph.D. degrees from the University of Paris VI in 1989 and 1993, respectively.

Since 1982 he has been with ENST Paris, France, as a lecturer in the Communications department. He is currently engaged in research in the area of high speed optical communication systems.

Jacques Prado was born in 1948, in Rennes, France. He received the Ph.D. degree in electronics from the University of Paris XI, Orsay, France, in 1976.

Since 1976, he has been with the Signal Processing Department of ENST Paris, France, as a Teaching Researcher. His research interests are in digital filtering, automatic analysis of EEG signals, and real time implementation of signal processing algorithms on DSP's.

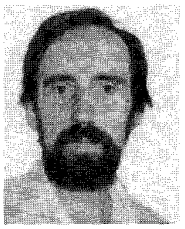

Robert Vallet was born in 1949 in France. He received the D.E.A. degree from the University of Paris XI, Orsay, France, in 1980 and the Ph.D. degree from ENST Paris, France, in 1991.

He has been with ENST Paris, France, since 1978. His research interests are in digital signal processing, blind equalization, and modulation schemes over time varying Rayleigh fading channels.

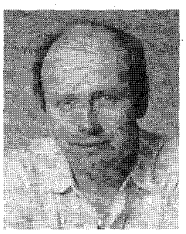

Philippe Gallion (M'90) was born in March 1950, in Saint-Dizier, France. He received the Maitrise and the Doctorat de Troisième Cycle from the University of Reims in 1972 and 1975, respectively, and the Doctorat d'Etat from the University of Montpellier in 1986.

Senior Lecturer at the University of Reims, his research involved Optical Signal Processing in Electron Microscopy. He joined ENST Paris, France in 1978 where he is currently Professor and Head of the Communication Department. He is lecturing in the fields of Electromagnetism, Optics, Quantum Electronics and Optical Communications and is in charge of the Mastère program in the field of optoelectronics and microwave devices. He is also lecturing at the University of Paris VI. His present research topics include noise, modulation and tunability of semiconductor lasers, optical injection-locking and advanced optical communication and switching techniques. He is author or co-author of more than 90 technical papers and communications.

Dr. Gallion is a member of the Optical Society of America.